

Effects of an off-center donor impurity on the electronic and optical properties of a spherical ZnO/ZnS multi-shell quantum dot with a parabolic potential

M. EL KHOU*, E. A. IBNOUELGHAZI, D. ABOUELAOUALIM

LN2E, Department of Physics, Faculty of Sciences Semlalia, Cadi Ayaad University, Marrakesh, Morocco

Within the framework of the effective mass approximation, the electronic and optical properties of an electron confined in a spherical ZnO/ZnS multi-shell Quantum dot confined in a parabolic potential are investigated. We carry on the numerical calculations using the finite difference method (FDM) in order to find the electron's energy eigenvalues and eigenstates, required in the computation of the binding energy for to the ground state and other excited states, in addition to the transition dipole moment (TDM) along the z-direction for the (1s) to (1p) transition state, under the influence of a perturbing potential corresponding to an off-center donor impurity, then we use all those parameters to compute the linear absorption coefficient for multiple impurity positions along the z-axis. The results show that the variation of the donor impurity's position does have an impact on the electronic and optical properties of the confined electron, even though all the other parameters are kept fixed.

(Received July 5, 2021; accepted February 11, 2022)

Keywords: Core/Shell/Shell/Shell Quantum dot, Parabolic potential, Off-center donor impurity, Finite difference method, Binding energy

1. Introduction

Quantum dot are zero-dimensional structures that are intermediate between solids and atoms, where the electron motion is restricted in all three dimensions granting them remarkably different optical properties in comparison with their bulk counterpart. They have gained considerable attention in recent years, due to their potential applications in optoelectronic and photonic devices [1–8]. The ab initio calculation of colloidal semiconductor QDs, such as DFT [9] and atomistic pseudopotential approach [10], has been performed to predict electronic and optical properties as a function of several structure parameters such as the size and material composition of the dot, however they require heavy mathematical and computational complexity [11–13] in comparison with the framework of the effective mass approximation (EMA) which provides reliable calculation results of the energies and wave functions of the electron/hole states [14].

Quantum dots are usually coated with one or multiple different semiconductor material with a wider bandgap in order to yield a layer that passivates surface defects and thus improves the luminescence efficiency [15]. Adding more layers to a single material quantum dot gives a greater active volume which increase the sensitivity of the nano-device [16]. In order to avoid the imperfections in such heterostructures like strain [17,18] which is induced by lattice mismatch at the interface, the material's crystal structure must be the same for all layers while the lattice constants should not differ by more than 12% to allow for the epitaxial growth of the shell [19].

Introducing a hydrogenic donor impurity can alter the electronic and optical properties of low-dimensional systems, as proven by the results shown in the earliest works regarding this subject made by Bastard and others [20,21]. Most theoretical works have been made on shallow donors in spherical QDs employing perturbation theory [22–26] or variational approaches [27–33], in addition to employing different confining potentials forms, such as the parabolic confinement potential [34,36], and rectangular parallelepiped shaped QD [37]. Several numerical methods were employed to solve the Schrodinger equation associated with a donor impurity in a multi-shell quantum dots, Boz et al. studied the binding energies of a spherical MSQD using a fourth-order Runge-Kutta method [38], while Şahin et al. carried out his calculation using the Shooting method [35], whereas Zeng et al. used the numerical potential morphing method (PMM) [39].

So many authors have reported the optical properties of a single electron confined in either a single or a multi-shell quantum dots MSQD, all cases are either under the influence of a donor impurity or without [39–41], while Yakar et al. investigated the optical and electronic properties of two-electron quantum dot confined first by an infinite spherical potential surface [42] then looked at the effects of a parabolic potential on the ground and excited energy states with the presence of an impurity inside an infinite spherical confining potential well [43].

In the present paper we carry out a detailed study of the electronic and optical properties of an MSQD with a parabolic confinement potential for cases with and without an off-center hydrogenic donor impurity. In this context,

the intersublevel linear absorption coefficient is calculated as a function of photon energy and layer thicknesses. For this purpose, the electronic energy levels and their wave functions are determined in the framework of the effective mass approximation using the finite difference method (FDM). The results are presented comparatively for cases with and without the donor impurity.

2. Theoretical framework

We present in this study an electron confined in an isolated spherical multi-shell quantum dot with a parabolic confining potential with the core radii R_1 and the well width with thickness Δ_2 both have ZnO material, whilst the barrier thickness Δ_1 and the coating layer thickness Δ_3 both host ZnS material with a greater energy gap compared to ZnO, as shown in Fig. 1.

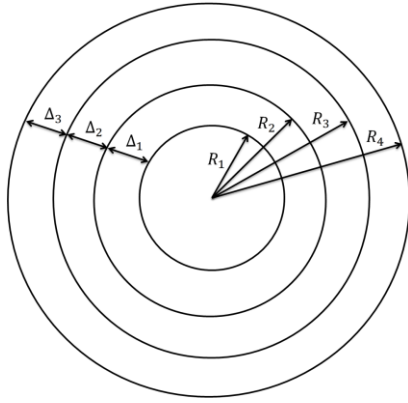


Fig. 1. Cross section of a spherical multi-shell quantum dot

Such system can be described by solving the unperturbed Hamiltonian with a position dependent effective mass which is given in the form suggested by BenDaniel and Duke [44]:

$$H_0 = -\frac{\hbar^2}{2} \nabla \frac{1}{m_e^*(r)} \nabla + V_p(r) \quad (1)$$

where the first term is the kinetic energy operator for a position dependent effective mass, while $V_p(r)$ is the parabolic confining potential [35], it can be written as follows:

$$V_p(r) = \begin{cases} V_0 \times \left(\frac{r}{R_1}\right)^2 & 0 \leq r \leq R_1 \\ V_0 & R_1 \leq r \leq R_2 \\ V_0 \times \left(\frac{r-p_0}{\Delta_2/2}\right)^2 & R_2 \leq r \leq R_3 \\ V_0 & R_3 \leq r \leq R_4 \\ \infty & r > R_4 \end{cases} \quad (2)$$

where $p_0 = \frac{R_2 + R_3}{2}$, and where V_0 is the band offset,

which is equal to the height of the barrier potential trapping the electrons inside ZnO surrounded by ZnS, it is in general defined as the difference between the lowest value of both material's conduction bands as long as their Fermi Level is aligned equally, since we are in the Thermodynamic equilibrium, which implies that no current flows throughout the hetero-structure, or we might use the Anderson rule despite its limitation, which require the knowledge of the electron affinity of each material [45].

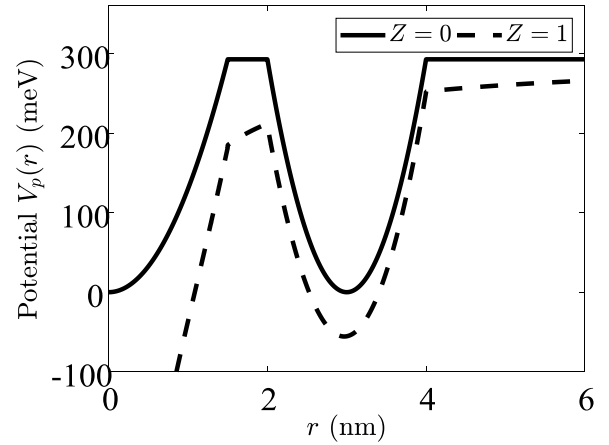


Fig. 2. ZnO/ZnS Multi-Shell Quantum dot with a parabolic confining potential with a narrow internal ZnS barrier thickness

The effective mass is defined in the same manner as:

$$m_e^*(r) = \begin{cases} m_1^* & 0 \leq r \leq R_1 \\ m_2^* & R_1 \leq r \leq R_2 \\ m_3^* & R_2 \leq r \leq R_3 \\ m_4^* & R_3 \leq r \leq R_4 \end{cases} \quad (3)$$

The Eigen states $|n^{(0)}\rangle$ are solutions of the unperturbed Hamiltonian H_0 satisfying:

$$H_0 |n^{(0)}\rangle = E_n^{(0)} |n^{(0)}\rangle \quad (4)$$

We generate the radial part of the unperturbed states $|n^{(0)}\rangle$ using the Finite Difference Method (FDM), while the angular part is represented by spherical harmonics.

The total Hamiltonian which contains the donor impurity as a perturbation is:

$$H_1 = H_0 + V(r) \quad (5)$$

where $V(r)$ is the perturbing symmetry, which is a donor impurity that can vary its position across the Multi-Shell Quantum dot, defined as follows:

$$V(\mathbf{r}) = -\frac{Ze^2}{4\pi\epsilon(\mathbf{r})|\mathbf{r}-\mathbf{r}_0|} \quad (6)$$

In spherical coordinates, the expansion of the Green's function is:

$$\frac{1}{|\mathbf{r}-\mathbf{r}_0|} = \sum_{\tau=0}^{\infty} \sum_{\gamma=-\tau}^{\tau} \frac{4\pi}{2\tau+1} \frac{1}{r^{\gamma}} \left(\frac{r^{\gamma}}{r^{\gamma}}\right)^{\tau} Y_{\tau\gamma}^*(\theta_0, \varphi_0) Y_{\tau\gamma}(\theta, \varphi) \quad (7)$$

where $(r_0, \theta_0, \varphi_0)$ are the coordinates of the donor impurity inside the CSSS Quantum dot, each coordinate is associated with a specific quantum number.

From here on we change the notation of the zeroth order states to the following $|n^{(0)}\rangle = |nlm\rangle$, in order to keep track of the different states we are working with. Then we calculate the zeroth order binding energy which is the expectation value of the potential $V(\mathbf{r})$ with states with the same quantum numbers, without taking account the magnetic quantum number m as follows:

$$E_{nlm}^b = -\langle nlm|V(\mathbf{r})|nlm\rangle \quad (8)$$

We can use the perturbed states to compute the first order binding energy, which is needed for the (s) electronic states, since the expectation value using (s) states gives less accurate results, in addition to not including any angular part. Gathering both energy values found in Eq. (4) and (8) will give us the total energy as follows:

$$E_{nlm} = E_{nlm}^{(0)} - E_{nlm}^b \quad (9)$$

In order to see the influence an off-center donor impurity hold over intraband transition in the conduction band, we need to calculate each corresponding transition's dipole moment (TDM), which give us an idea of either the transition is even possible to occur or how weak the transition is compare to other in the same vicinity, we need to use perturbed Eigen states, which are written up to the first order as:

$$|n\rangle = |n^{(0)}\rangle + \sum_{k \neq n} \frac{\langle k^{(0)}|V(\mathbf{r})|n^{(0)}\rangle}{E_n^{(0)} - E_k^{(0)}} |k^{(0)}\rangle \quad (10)$$

Thus by using Eq. (10) we can write the transition dipole moment (TDM) along the direction z as follows:

$$M_{n \rightarrow m}^z = \langle m|z|n\rangle \quad (11)$$

Eq. (11) can be expressed with respect to the unperturbed states up to the first order as follows:

$$\begin{aligned} M_{n \rightarrow m}^z &= \langle m^{(0)}|z|n^{(0)}\rangle + \\ &\sum_{k \neq n} \frac{\langle k^{(0)}|V(\mathbf{r})|n^{(0)}\rangle}{E_n^{(0)} - E_k^{(0)}} \langle m^{(0)}|z|k^{(0)}\rangle + \\ &\sum_{k \neq m} \frac{\langle m^{(0)}|V(\mathbf{r})|k^{(0)}\rangle}{E_m^{(0)} - E_k^{(0)}} \langle k^{(0)}|z|n^{(0)}\rangle \end{aligned} \quad (12)$$

Evaluating Eq. (12) for a $(n_1 00)$ to $(n_2 10)$ transition can be expressed as follows:

$$\begin{aligned} M_{n_1 00}^{n_2 10} &= \frac{1}{\sqrt{3}} \langle n_2 10|r|n_1 00\rangle + \\ &\frac{1}{\sqrt{3}} \sum_{n \neq n_1} \frac{\langle n 00|V(\mathbf{r})|n_1 00\rangle}{E_{n_1 00}^{(0)} - E_n^{(0)}} \langle n_2 10|r|n 00\rangle + \\ &\frac{1}{\sqrt{3}} \sum_{n \neq n_2} \frac{\langle n_2 10|V(\mathbf{r})|n 10\rangle}{E_{n_2 10}^{(0)} - E_n^{(0)}} \langle n 10|r|n_1 00\rangle + \\ &\frac{2}{\sqrt{15}} \sum_{n=1} \frac{\langle n 20|V(\mathbf{r})|n_1 00\rangle}{E_{n_1 00}^{(0)} - E_n^{(0)}} \langle n_2 10|r|n 20\rangle \end{aligned} \quad (13)$$

The linear Absorption coefficient is given as follows:

$$\alpha(\omega) = \frac{\omega}{n_r \epsilon_0 c} \text{Im}(\epsilon_0 \chi_e^{(1)}(\omega)) \quad (14)$$

where $\chi_e^{(1)}(\omega)$ is the first order electric susceptibility in the frequency domain, it can be obtained by solving a two level system master equation, using a perturbing electric field with frequency ω , it can written as follows:

$$\epsilon_0 \chi_e^{(1)}(\omega) = \frac{\sigma_v |M_{12}|^2}{\hbar\omega_{12} - \hbar\omega - i\hbar\Gamma_{12}} \quad (15)$$

where M_{if} is the Transition dipole moment chosen along the z-direction, from an initial state (i) to a final state (f), induced by the external electric field polarized in the same direction, it's given as follows:

$$M_{if} = -eM_{if}^z \quad (16)$$

while Γ_{if} is the inverse of the state's lifetime, given as the off diagonal eigenvalue of the Hermitian damping operator $\hat{\Gamma}$, given as follows:

$$\Gamma_{if} = \langle f|\hat{\Gamma}|i\rangle \quad (17)$$

And is the charge carrier density, and n_r is the refractive index and c is the speed of light.

3. Results and discussion

In order to figure out the effects of shifting the donor impurity off the center along the z-direction ($\theta_0=0$) on the electronic and optical properties of an electron confined in a Multi-Shell quantum dot with a parabolic potential, we compute the unperturbed wave function using the finite difference method, which we'll be using as basis for computing the expectation values required in the perturbation method, we take all the parameters from this reference [39], starting with the offset potential which is chosen to be $V_0=292.8\text{meV}$, as for the electron density $\sigma_v=1.7\times 10^{24}\text{m}^{-3}$, the relaxation time $T_{12}=1\text{ps}$, and the refractive index is $n_r=2.9629$, the relative dielectric constants of ZnO and ZnS, respectively $\epsilon_1=\epsilon_3=8.66\epsilon_0$, $\epsilon_2=\epsilon_4=8.9\epsilon_0$, where ϵ_0 is the vacuum permittivity. The electron effective mass is taken to be $m_1^*=m_3^*=0.265m_0$ and $m_2^*=m_4^*=0.24m_0$, where m_0 is the free electron mass.

All probability densities considered in this simulation are concentrated around the z-axis since the magnetic quantum number m is taken to be zero, with the exception of the (s) states which have a spherical symmetry, we will carry out the computation using two values of the interior ZnO barrier thickness Δ_1 , first we take a small thickness equal to $\Delta_1=0.5\text{nm}$ then we change it to a slightly bigger value $\Delta_1=1.25\text{nm}$ while keeping the ZnO well thickness around $\Delta_2=2.0\text{nm}$ and fixing the outer ZnS shell at $\Delta_3=2\text{nm}$, to prevent the electron from escaping outside of the dot, while fixing the outer radius of the MSQD at $R_4=6\text{nm}$, which means that the part added to ZnS barrier thickness is taken from the core radii R_1 and vice versa.

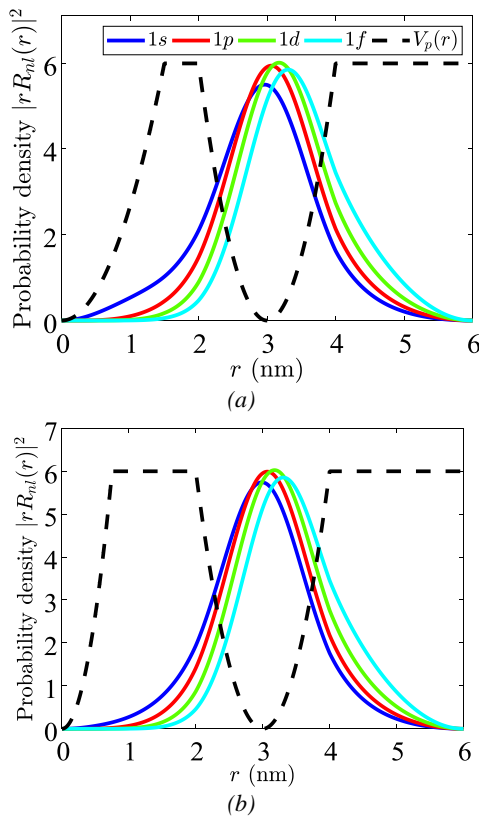


Fig. 3. Unperturbed probability density for $n=1$ while (a) $\Delta_1=0.5\text{nm}$ (b) $\Delta_1=1.25\text{nm}$ (color online)

Fig. 3 gives us the ground level ($n=1$) electron's probability density for an electron confined in a MSQD with a parabolic potential, for a couple of ZnS barrier thicknesses of 0.5nm and 1.25nm , first we take the ZnS barrier's thickness equal to $\Delta_1=0.5\text{nm}$ which is shown in Fig. 3(a), for the ground state (1s), we see that there's a high probability density both at the core and the well with a lower value at the interface between them, which is due to quantum tunneling, since the electron doesn't have the minimum energy required to escape the well, as we make ℓ different than zero, we observe that the probability density shift to the right away from the center, with an increase in the magnitude of the probability density as shown in Fig. 3(a), as a good amount of the probability once reside at the core ZnO transferred to ZnO well, it's worth noting that the first three states (1s), (1p) and (1d) with confinement energy respectively 174.76meV , 218.24meV and 286.16meV are all situated in the ZnO well with a thickness of 2nm , they all lack energy necessary in order to escape the well, which is surrounded by ZnS barriers with a height of 292.8meV , however the fourth state (1f) have an energy which surpasses the height of the well about 374.43meV , which can be confirmed by Fig. 3(a) since most of the probability density is located at the third ZnO/ZnS interface.

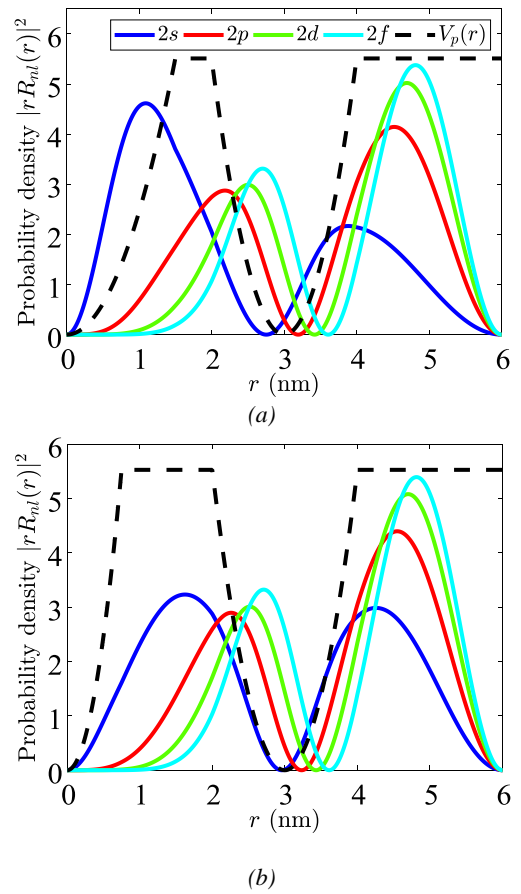


Fig. 4. Unperturbed probability density for $n=2$ while (a) $\Delta_1=0.5\text{nm}$ (b) $\Delta_1=1.25\text{nm}$ (color online)

As we thicken the ZnS barrier to $\Delta_1=1.25\text{nm}$, we observe that the ground state probability density have dropped noticeably at the core ZnO, as the probability of quantum tunneling gets exponentially smaller when the barrier gets larger, thus the electron needs to rely only on the energy gained by confinement effect in order to spread the probability density across the quantum dot, which is about 179.25meV for the (1s) state, definitely less than the barrier height, the same thing can be said about the (1p) and the (1d) states with energy respectively about 219.62meV and 286.71meV , even though they benefit an energy increase because of to the built-in spherical potential, they get pushed away from the center as a consequence, which render their bound state considerably weaker, the (1f) state electron possess energy higher than the built in potential, about 374.64meV , however it also moves away from the center. As the electron get excited to the second principal energy level ($n=2$), we observe an increase in the confinement energy of the electron,

packaged with its corresponding probability density distribution, which is split between two specific points where the highest density is always closer to the center, we see from Fig. 4 that the only apparent change in any state triggered by a change in the barrier thickness is displayed by the (2s) state and some minor differences for the (2p) state, we observe that the majority of the probability density is located at the core material for both barrier thicknesses for (2s) state, however when $\Delta_1=0.5\text{nm}$ we see a further increase in the probability density at the center while the confinement energy decrease to 380.21meV when we compare it with the case where $\Delta_1=1.25\text{nm}$ in which the energy equal to 421.52meV . We observe a somewhat similar behavior for the (2p) state, as we see an increase in the magnitude of the probability density toward the center of the dot, and a slight lowering of energy from 491.28meV to 484.11meV when we reduce the thickness Δ_1 from 1.25nm to 0.5nm .

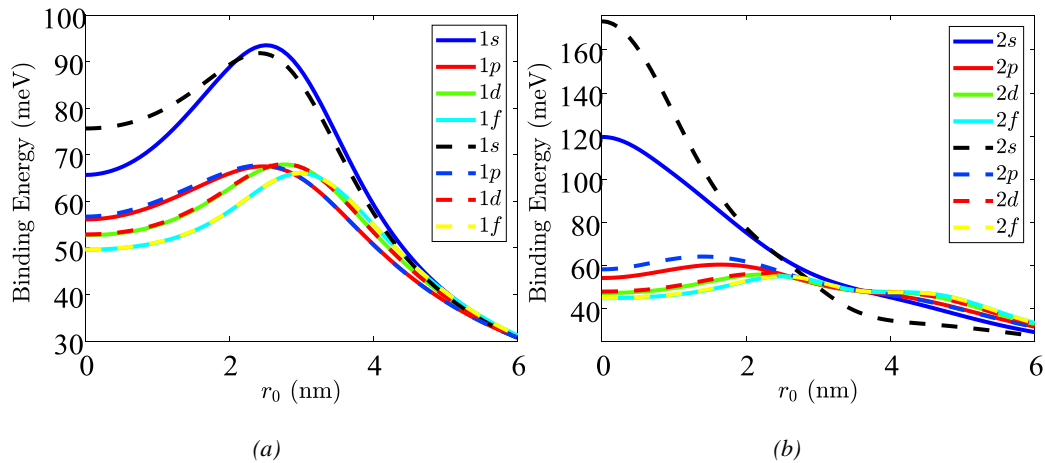


Fig. 5. Variation of multiple states Binding Energy for a $R_4=6\text{nm}$ Multi-Shell Quantum dot, when $\Delta_1=0.5\text{nm}$ (dash lines) and $\Delta_1=1.25\text{nm}$ (continuous lines) (color online)

Fig. 5 shows the variation of the binding energy as a function of the impurity's position along the z-direction for two different ZnS barrier thicknesses, first we tackle the case when the barrier thickness equal to $\Delta_1=1.25\text{nm}$ (straight line), then we compare it to the other case where $\Delta_1=0.5\text{nm}$ (dash line), when we start off with the ground level ($n=1$) given in Fig. 5(a), we observe that the ground state energy start with a high binding energy value around 65.68meV when compared to the other excited states, as we begin to shift the impurity away from the center, we see a smooth energy increase for all states, especially a significant one for the ground state (1s), this behavior can be explained by comparing the position where the probability density peaks for all corresponding states with the points where the binding energy summit, we see in Fig. 3(b) that the highest probability density is located in the $\Delta_2=2\text{nm}$ ZnO well region, which indicate an interaction occurrence between the impurity and the electron density in that layer, which rises the binding energy to a maximal value of 93.54meV , 67.52meV , 67.93meV and 66.05meV respectively for the (1s), (1p), (1d) and (1f), as we keep

moving the impurity away from the center the binding energy decrease steadily until it reaches the lowest value possible which is roughly about 31meV for all the states. We observe a different scenario when ($n=2$) as we see that the (2s) state start off with a maximum binding energy around 119.7meV , since the probability density mostly centered, then grow smaller as we move the impurity away from the center, the other case when ℓ is different than zero, the probability density get pushed away from the center, which explains the overall weak binding energies at the center, since they only reach a peak value of 60.47meV for the (2p) and 55.89meV for (2d) and 55.05meV for the (2f) state, then follows by a decrease in the binding energy as we move the impurity with a slight increase since we have two peak values in the probability density, which is slightly clear in the (2d) and (2f).

As we reduce the internal ZnS barrier's thickness to $\Delta_1=0.5\text{nm}$, majority of states considered in this study remain to some extent invariant except for this particular states (1s), (2s) and (2p), as we can see in Fig. 5, they experience a binding energy increase especially at the core

ZnO, most drastic change is experienced by the states with zero angular momentum, the ground state's (1s) binding energy increased to 75.65meV at the center and peaked at 91.84meV when $r_0=2.42\text{nm}$, while the (2s) state reached a maximum value of 173.29meV at the center core, as for the (2p) state which increased to 58.28meV at the center and peaked at 64.21meV around $r_0=1.41\text{nm}$, all other states experienced a miniscule binding energy increase which is difficult to spot on, since the dash lines which correspond to $\Delta_1=0.5\text{nm}$ are nearly on top of the continuous curves which belongs to the case where $\Delta_1=1.25\text{nm}$, this behavior can be further understood by comparing it with the probability density previously mentioned in Figs. 3 and 4, we can say briefly that if the barrier thickness Δ_1 is reduced, the probability of electron tunneling through the barrier increases exponentially, which allows for extra states beyond the barrier despite the lack of energy.

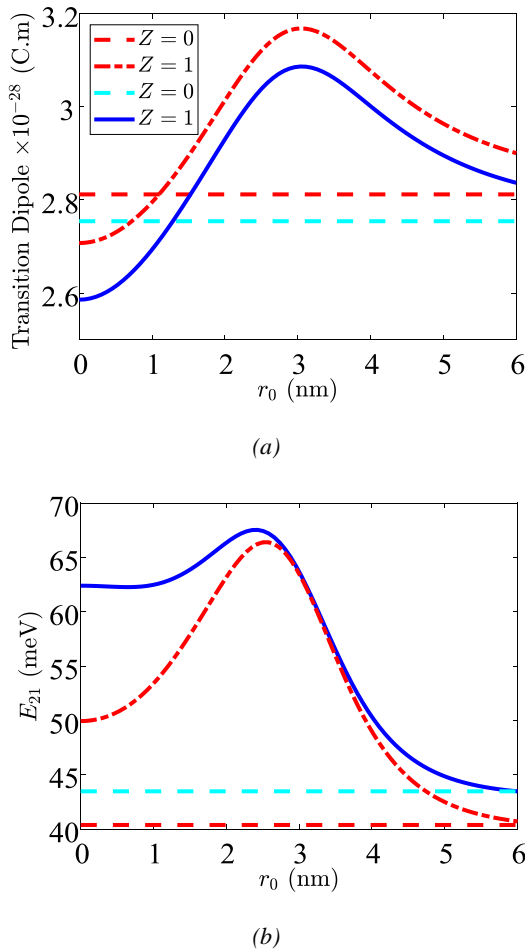


Fig. 6. Variation of (a) the absolute Value of the perturbed Transition Dipole Moment (b) the energy difference E_{21} , for the (1s) to (1p) transition when $\Delta_1=0.5\text{nm}$ (dark blue and light blue) and $\Delta_1=1.25\text{nm}$ (red and brown) (color online)

Next we look at a crucial parameter required to the computation for optical properties, such as the absorption coefficient (AC), which is the transition dipole moment briefly noted TDM, given in Fig. 6(a) as a function of the

donor impurity's position, the transition in question here in this paper is a (1s) to (1p) state transition for a couple values of ZnS barrier's thickness, while including the impurity-less case shown as a constant dash line as a reference, we observe at first glance that the overall value of the TDM when the ZnS barrier width equal to $\Delta_1=1.25\text{nm}$ is noticeably superior to the case when the barrier thickness is reduced to 0.5nm, this fact even holds when the donor impurity is absent from the quantum dot, aside from that we see that both cases vary in the same manner when we shift the impurity away from the center, we see that as soon as we introduce the impurity at the center of the dot, we see a reduction in the magnitude of the TDM, however just as we start moving the impurity from the center we observe a rising in the TDM magnitude and maxing out as we reach the neighborhood of $r_0=3.0\text{nm}$, right after that it follows by a diminishing in its value as the impurity gets further away from the high probability density positions which make the value of the TDM to converge gradually toward the vicinity of the impurity-less case.

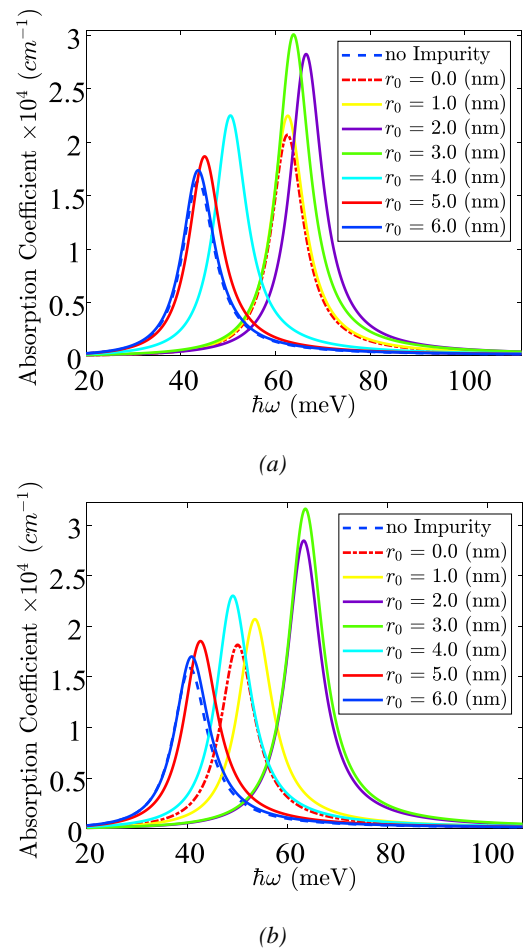


Fig. 7. Linear Absorption coefficient for a (1s) to (1p) transition for (a) $\Delta_1=0.5\text{nm}$ (b) $\Delta_1=1.25\text{nm}$ (color online)

Fig. 7 shows variation of positions which the linear absorption peaks (AC) takes as a function of the impurity position along the z-direction for a transition state from (1s) to (1p), we consider for the first case a barrier

thickness of $\Delta_1=0.5\text{nm}$ given in Fig. 7(a) as we introduce the impurity at the center, the (AC) peak exhibit a blue-shift while its magnitude rises up, however as we start to move the impurity away from the center we see a slight red shift as the energy difference decrease with a very small amount as we see in Fig. 6(b) (blue curve), as we keep moving the impurity the difference of energy keep increasing until summiting around 67.54meV at $r_0=2.4\text{nm}$, then we see a red shift with a magnitude increase since the TDM keep increasing and reach a maximum value at $r_0=3\text{nm}$ as we see in Fig. 6(a) (blue curve), if we continue moving the impurity pass 3nm the energy difference decrease with a lowering of the magnitude converging to the value of the impurity-less case. As we make the barrier thickness a bit wider equal to $\Delta_1=1.25\text{nm}$, we observe that the overall magnitude of TDM get higher than the previous case, while the energy difference decreases noticeably both at the center and the edge of the dot, which create a more apparent blue-shift as we vary the radius of the impurity from the center of the dot until $r_0=2.54\text{nm}$ reaching a maximum difference of 66.41meV as shown in Fig. 6(b) (red dashed curve), when we surpasses this value we observe a red-shift with a magnitude decrease while converging to the case with no impurity both energy-wise and TDM-wise as we reach the edge of the dot.

4. Conclusion

In this study, the Binding energy, transition dipole moment (TDM) and the linear absorption coefficient (AC) for a ZnO/ZnS multi-shell spherical quantum dot under the influence of an off-center donor impurity have been investigated, using the compact-density matrix formalism and an iterative method for the time dependent perturbing AC potential in the electric dipole approximation, then by using perturbed eigenstate computed by the static non degenerate perturbation method generated by the off-center impurity potential within the effective mass approximation, we have calculated the binding energy for the ground state and several excited states while varying the coordinates of the donor impurity, furthermore we computed the variation of the transition dipole moment as a function of the position of the off-center donor impurity, finally we use all those results to calculate the absorption coefficient, all computations done have been made with two distinctive values of the ZnS interior barrier thickness. We have shown that the position of the donor impurity is capable of modifying the electronic and optical properties of Multi shell Quantum dot, while keeping the dot size fixed.

References

[1] L.-C. Chen, Y.-H. Tien, J. Tian, *J. Alloys Compd.* **892**, 162140 (2022).
 [2] Y. Kim, S. Ham, H. Jang, J. H. Min, H. Chung, J. Lee, D. Kim, E. Jang, *ACS Appl. Nano Mater.* **2**, 1496 (2019).

[3] W. A. A. Mohamed, H. Abd El-Gawad, S. Mekkey, H. Galal, H. Handal, H. Mousa, A. Labib, *Nanotechnol. Rev.* **10**, 1926 (2021).
 [4] Y. Shu, X. Lin, H. Qin, Z. Hu, Y. Jin, X. Peng, *Angew. Chem. Int. Ed.* **59**, 22312 (2020).
 [5] D. Bederak, D. M. Balazs, N. V. Sukharevska, A. G. Shulga; M. Abdu-Aguye, D. N. Dirin, M. V. Kovalenko, M. A. Loi, *ACS Appl. Nano Mater.* **1**, 6882 (2018).
 [6] J. Zhang, J. Jin, J. Wan, S. Jiang, Y. Wu, W. Wang, X. Gong, H. Wang, *Chem. Eng. J.* **408**, 127351 (2021).
 [7] A. Bokare, J. Arif, F. Erogbogbo, *Nanomaterials* **11**, 2211 (2021).
 [8] X. Xu, L. Zhou, D. Ding, Y. Wang, J. Huang, H. He, Z. Ye, *ACS Appl. Nano Mater.* **3**, 538 (2020).
 [9] S. K. Haram, A. Kshirsagar, Y. D. Gujarathi, P. P. Ingole, O. A. Nene, G. B. Markad, S. P. Nanavati, *J. Phys. Chem. C*, **115**, 6243, (2011).
 [10] J.-W. Luo, G. Bester, A. Zunger, *Phys. Rev. B* **79**, 125329 (2009).
 [11] A. Mielnik-Pyszczorski, K. Gawarecki, P. Machnikowski, *Sci. Rep.* **8**, 2873 (2018).
 [12] O. Rubel, F. Tran, X. Rocquefelte, P. Blaha, *Comput. Phys. Commun.* **261**, 107648 (2021).
 [13] M. Pedersen Lohne, G. Hagen, M. Hjorth-Jensen, S. Kvaal, F. Pederiva, *Phys. Rev. B* **84**, 115302 (2011).
 [14] H. Yeo, J. S. Lee, M. E. Khan, H. S. Kim, D. Y. Jeon, Y.-H. Kim, *J. Phys. Mater.* **3**, 034012 (2020).
 [15] B. O. Dabbousi, J. Rodriguez-Viejo, F. V. Mikulec, J. R. Heine, H. Mattoussi, R. Ober, K. F. Jensen, M. G. Bawendi, *J. Phys. Chem. B* **101**, 9463 (1997).
 [16] S. Ortakaya, M. Kirak, *Chin. Phys. B* **25**, 127302 (2016).
 [17] J. T. L. Gamler, A. Leonardi, X. Sang, K. M. Koczur, R. R. Unocic, M. Engel, S. E. Skrabalak *Nanoscale Adv.* **2**, 1105 (2020).
 [18] T. E. Pahomi, T. O. Cheche, *Chem. Phys. Lett.* **612**, 33 (2014).
 [19] P. Reiss, M. Protière, L. Li, *Small* **5**, 154 (2009).
 [20] M. Şahin, *Phys. Rev. B* **77**, 045317 (2008).
 [21] G. Bastard, *Phys. Rev. B* **24**, 4714 (1981).
 [22] C. Bose, *Physica E* **4**, 180 (1999).
 [23] C. Bose, C. K. Sarkar, *Solid State Electron.* **42**, 1661 (1998).
 [24] C. Bose, C. K. Sarkar, *Physica B* **253**, 238 (1998).
 [25] C. Bose, C. K. Sarkar, *Phys. Stat. Sol. B* **218**, 461 (2000).
 [26] J. H. Yuan, C. Liu, *Physica E* **41**, 41 (2008).
 [27] C. Bose, *J. Appl. Phys.* **83**, 3089 (1998).
 [28] J.-L. Zhu, J.-H. Zhao, J.-J. Xiong, *J. Phys. Condens. Matter* **6**, 5097 (1994).
 [29] A. J. Peter, *Physica E* **28**, 225 (2005).
 [30] S. Kang, J. Li, T.-Y. Shi, *J. Phys. B: At. Mol. Opt. Phys.* **39**, 3491 (2006).
 [31] A. K. Manaselyan, A. A. Kirakosyan, *Physica E* **28**, 462 (2005).
 [32] C. Dane, H. Akbas, S. Minez, A. Guleroglu, *Physica E* **41**, 278 (2008).

- [33] Y. Yakar, B. Çakır, A. Özmen, *Commun. Theor. Phys.* **53**, 1185 (2010).
- [34] E. M. Kazaryan, L. S. Petrosyan, H. A. Sarkisyan, *Physica E* **16**, 174 (2003).
- [35] M. Şahin, K. Koksal, *Semicond. Sci. Technol.* **27**, 125011 (2012).
- [36] Y. Yakar, B. Çakır, A. Özmen, *Superlattices and Microstructures* **60**, 389 (2013).
- [37] S.-S. Li, J.-B. Xia, *J. Appl. Phys.* **101**, 093716 (2007).
- [38] F. K. Boz, S. Aktas, A. Bilekkaya, S. E. Okan, *Appl. Surf. Sci.* **256**, 3836 (2010).
- [39] Z. Zeng, C.S. Garoufalis, A. F. Terzis, S. Baskoutas, *J. Appl. Phys.* **114**, 023510 (2013).
- [40] K. S. Rahul, N. Devaraj, R. K. Babu, S. Mathew, K. Salini, V. Mathew, *J. Phys. Chem. Solids* **106**, 99 (2017).
- [41] H. Tas, M. Şahin, *J. Appl. Phys.* **112**, 053717 (2012).
- [42] Y. Yakar, B. Çakır, A. Özmen, *Comput. Phys. Commun.* **188**, 88 (2015).
- [43] Y. Yakar, B. Çakır, A. Özmen, *Philosophical Magazine* **95**, 311 (2015).
- [44] D. J. Ben Daniel, C. B. Duke, *Phys. Rev.* **152**, 683 (1966).
- [45] R. L. Anderson, *IBM J. Res. Dev.* **4**, 283 (1960).

*Corresponding author: elkhmourad@gmail.com